ADP-induced rocking of the kinesin motor domain revealed by single-molecule fluorescence polarization microscopy

Hernando Sosa[1,2], Erwin J.G. Peterman[3,4], W.E. Moerner[3] and Lawrence S.B. Goldstein[1,5]

[1]Department of Cellular and Molecular Medicine and Howard Hughes Medical Institute, University of California San Diego, La Jolla, California 92093-0683, USA. [2]Present address: Department of Physiology and Biophysics, Albert Einstein College of Medicine, Bronx, New York 10461, USA. [3]Department of Chemistry, Stanford University, Stanford, California 94305-5080, USA. [4]Present address: Division of Physics and Astronomy, Vrije Universiteit, Amsterdam, The Netherlands. [5]Department of Pharmacology, University of California San Diego, La Jolla, California 92093-0683, USA.

Kinesin is an ATP-driven molecular motor protein that moves processively along microtubules. Despite considerable research, the detailed mechanism of kinesin motion remains elusive. We applied an enhanced suite of single- and multiple-molecule fluorescence polarization microscopy assays to report the orientation and mobility of kinesin molecules bound to microtubules as a function of nucleotide state. In the presence of analogs of ATP, ADP-Pi or in the absence of nucleotide, the kinesin head maintains a rigid orientation. In the presence of ADP, the motor domain of kinesin, still bound to the microtubule, adopts a previously undescribed, highly mobile state. This state may be general to the chemomechanical cycle of motor proteins; in the case of kinesin, the transition from a highly mobile to a rigid state after ADP release may contribute to the generation of the 8 nm step.

Kinesin, an essential cellular motor protein, uses the energy of ATP hydrolysis to move many steps (8 nm displacements between tubulin binding sites) along a microtubule without detachment[1]. Recently, a variety of data led to the proposal that a zipper-like conformational change in the 'neck linker' region of the kinesin motor domain occurs upon ATP binding[2]. Whether this change by itself can generate the observed 8 nm steps[3] or whether additional conformational changes contribute as well are questions of critical interest.

Bulk fluorescence polarization anisotropy measurements of kinesin in solution were used to detect changes in the overall shape of the molecule[4]. However, this method cannot detect changes in the relative orientation of kinesin with its microtubule track. Recently, the development of new biophysical assays based on observing the fluorescence of a single small dye molecule allows measurements without ensemble averaging and thus can resolve inhomogeneity due to different static and/or dynamical states[5–7]. One of these assays, fluorescence polarization spectroscopy of single fluorophores, was applied to study DNA conformation[8], the rotation of F1-ATPase[9] and the actomyosin system[10]. We developed an enhanced suite of single- and multiple-molecule fluorescence polarization microscopy assays and have applied these to study the kinesin problem, thus reporting the orientation and mobility of kinesin molecules bound to microtubules for the first time.

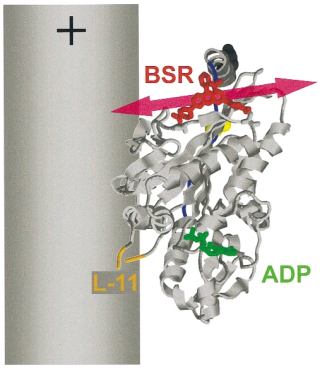

Fig. 1 Probe location and orientation. The fluorophore bis-((N-iodoacetyl)piperazinyl) sulfonerhodamine (BSR) (Molecular Probes) was docked into the rat kinesin structure[28] by placing its two reactive groups at the β-carbon positions of amino acids 169 and 174. The red arrow indicates the orientation of the BSR transition dipole moment. The position of the ADP molecule (green), loop 11 (L-11, orange) and BSR molecule (red) are indicated. In this view the neck linker region (blue), N-terminal (yellow) and C-terminal (black) regions are on the back of the molecule. The relative orientations of the kinesin motor domain and the microtubule are according to a proposed docking model based on cryo-electron microscopy[13]. Although three alternative microtubule–kinesin docking models have been proposed[15], they differ mainly on the azimuthal orientation (the angle around an axis centered on the motor and parallel to the microtubule long axis) of the motor head. Therefore all three predict a near perpendicular orientation for the probe dipole. However in one model[29] the probe on our labeled construct, KMC2–BSR would be facing the microtubule, possibly interfering with binding. This model then seems inconsistent with the observation that KMC2–BSR binds to microtubules and have normal microtubule-stimulated ATPase activity (see Methods). The docking orientation shown has been further supported by using gold labels[2].

The attachment of a bifunctional fluorophore to two residues of the protein structure orients the transition dipole so it can accurately mimic the orientation of the kinesin head relative to the microtubule[11]. Although the relative orientation is static and similar for almost all of the possible nucleotide states, in the ADP-bound form we discovered a previously unidentified state in which the head remains attached to the microtubule but rocks back and forth.

Fluorescent probe location and orientation

The kinesin construct (KMC2) used in this analysis is derived from the first 349 residues of the human kinesin heavy chain, but with only two cysteines located in the β5–α3 region defined in the kinesin crystal structure[12]. This monomeric construct includes the motor domain and neck linker but not the dimerization domain. We labeled KMC2 with a bifunctional thiol reactive rhodamine derivative, bis-((N-iodoacetyl)piperazinyl) sulfonerhodamine (BSR). According to the docking model of kinesin motors and microtubules[13], the kinesin motor domain in the presence of AMP-PNP (a nonhydrolysable analog of ATP) orients so that a bifunctional dipole (BSR) attached at the indicated residues (169 and 174) places the transition dipole almost perpendicular to the microtubule long axis and nearly parallel to the radial direction from the microtubule center (Fig. 1).

To determine the orientation of KMC2–BSR while bound to microtubule bundles found in cilia and flagella, we used laser light with alternating perpendicular polarization axes to excite KMC2–BSR molecules bound to axonemes (microtubule bundles found in cilia and flagella) and imaged the emitted fluores-

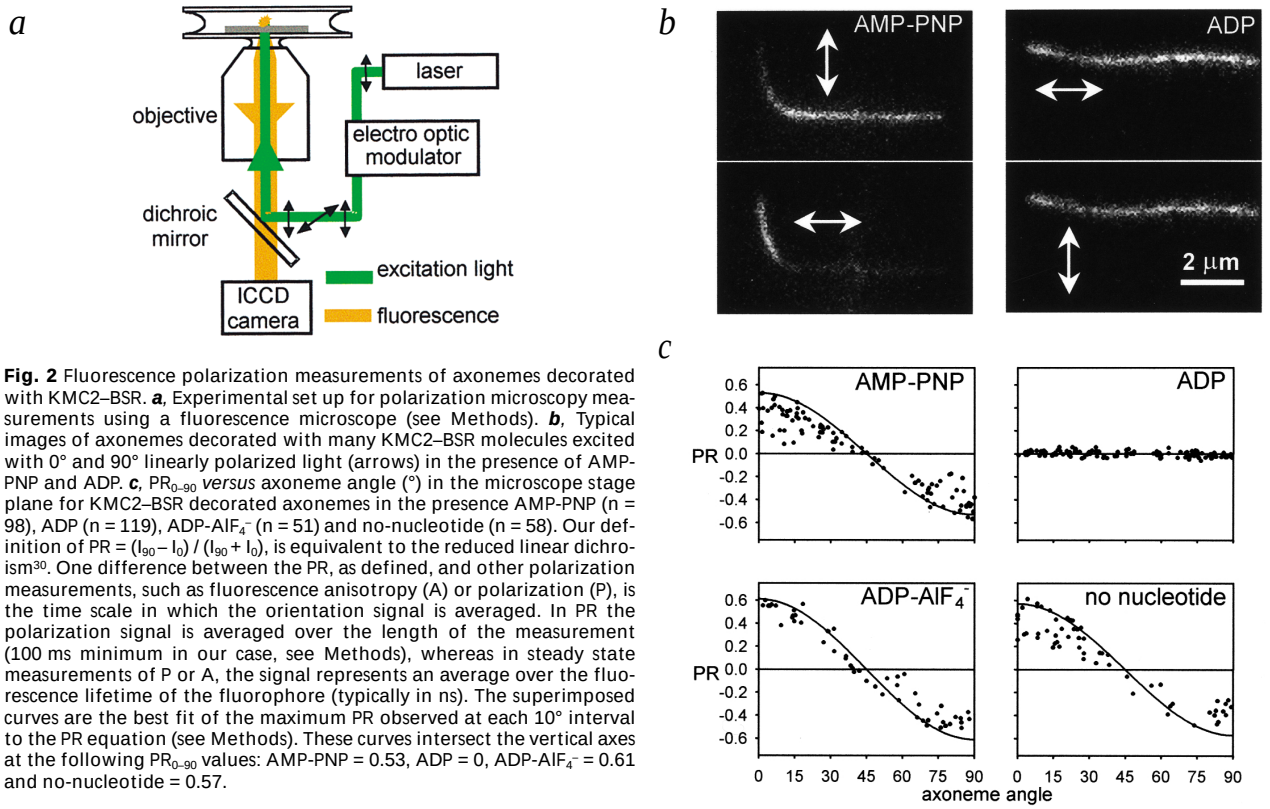

Fig. 2 Fluorescence polarization measurements of axonemes decorated with KMC2–BSR. ***a***, Experimental set up for polarization microscopy measurements using a fluorescence microscope (see Methods). ***b***, Typical images of axonemes decorated with many KMC2–BSR molecules excited with 0° and 90° linearly polarized light (arrows) in the presence of AMP-PNP and ADP. ***c***, $PR_{0–90}$ *versus* axoneme angle (°) in the microscope stage plane for KMC2–BSR decorated axonemes in the presence AMP-PNP (n = 98), ADP (n = 119), ADP-AlF_4^- (n = 51) and no-nucleotide (n = 58). Our definition of PR = $(I_{90} - I_0) / (I_{90} + I_0)$, is equivalent to the reduced linear dichroism[30]. One difference between the PR, as defined, and other polarization measurements, such as fluorescence anisotropy (A) or polarization (P), is the time scale in which the orientation signal is averaged. In PR the polarization signal is averaged over the length of the measurement (100 ms minimum in our case, see Methods), whereas in steady state measurements of P or A, the signal represents an average over the fluorescence lifetime of the fluorophore (typically in ns). The superimposed curves are the best fit of the maximum PR observed at each 10° interval to the PR equation (see Methods). These curves intersect the vertical axes at the following $PR_{0–90}$ values: AMP-PNP = 0.53, ADP = 0, ADP-AlF_4^- = 0.61 and no-nucleotide = 0.57.

cence (Fig. 2*a*). We first imaged axonemes decorated with many KMC2–BSR molecules (Fig. 2*b*). The images obtained in the presence of AMP-PNP displayed a strong anisotropy. When the exciting light was perpendicular to the microtubule axes, more light was emitted as expected, because light perpendicular to the microtubule will be aligned with the fluorophore dipole (Fig. 1).

To quantify this polarization anisotropy we calculated a ratio $PR_{0–90} = (I_{90} - I_0) / (I_{90} + I_0)$, where I_{90} and I_0 are the total light emitted with excitation light polarized at 90° or 0°, respectively, in the plane of the microscope stage. $PR_{0–90}$ was measured for many KMC2–BSR decorated axonemes in random orientations in the presence of different nucleotide species (Fig 2*c*). Each measurement corresponds to the added fluorescence signal of >1,000 KMC2–BSR molecules. For each nucleotide state we also calculated the expected $PR_{0–90}$ for an ensemble of fluorophores with cylindrical symmetry about the axoneme and a given angle with the microtubule long axis, axial angle (superimposed curves), chosen to fit the maximum $PR_{0–90}$ observed. Various nonideal effects, such as local distortions of the decorated microtubule structure, would lower the observed $PR_{0–90}$ values. Therefore, we concentrated on the highest observed values within each 10° range. In the case of AMP-PNP, the calculated curve corresponds to a dipole axial angle of 74° (see Methods) from the microtubule axis. This value is within the range expected from the docking of kinesin motors to microtubules[13] (Fig. 1).

In the absence of added nucleotides (apyrase present) or in the presence of ADP-AlF_4^- (thought to mimic the ADP-Pi state), only small angular changes were detected. The fitted curves (Fig. 2*c*) correspond to a dipole axial angle of 74°, 76° and 77° for the AMP-PNP, no-nucleotide and ADP-AlF_4^- states, respectively (assuming the same amount of rapid probe wobble for these three nucleotide states). Consistent with cryo-electron microscopy data, these results indicate a similar configuration for the microtubule-attached kinesin motor in these three nucleotide states[2,14,15].

The ADP-bound state of kinesin

In contrast to the AMP-PNP, ADP-AlF_4^- and no-nucleotide states, in the presence of ADP all $PR_{0–90}$ are close to 0 (Fig. 2*c*). This lack of polarization anisotropy can have three causes: (i) the axial angle of fluorescence dipoles has shifted to 54.7°, which leads to cancellation of the anisotropy from the cylindrical average around the axoneme; (ii) the dipoles are in random but fixed orientations; or (iii) the dipoles are highly mobile on the time scale of the measurement.

Measurements on single kinesin motors bound to axonemes allowed us to differentiate between these possibilities. In contrast to the near uniform fluorescence emission along the axoneme seen at higher concentrations (Fig. 2*b*), reduced kinesin concentrations in the assay displayed a line of individual fluorescent spots (Fig. 3*a*). Time courses of the fluorescence intensities from these spots (Fig. 3*b*) revealed constant intensity values with discrete photobleaching events, typical of single-molecule recordings[16]. To differentiate whether the low $PR_{0–90}$ value for a particular molecule was caused by probe mobility or by unfavorable orientation — that is, 45° from either polarization axis — we added two additional excitation polarization axes at 45° and 135°. These conditions allowed us to calculate an additional PR measure, $PR_{45–135}$. For an immobile dipole the relationship between $PR_{0–90}$ and $PR_{45–135}$ is fixed regardless of the dipole orientation because of the constant angle (45°) between the two pairs of axes. An immobile dipole will always satisfy the relationship $r = (PR_{0–90}^2 + PR_{45–135}^2)^{1/2} = 1$. A more mobile dipole

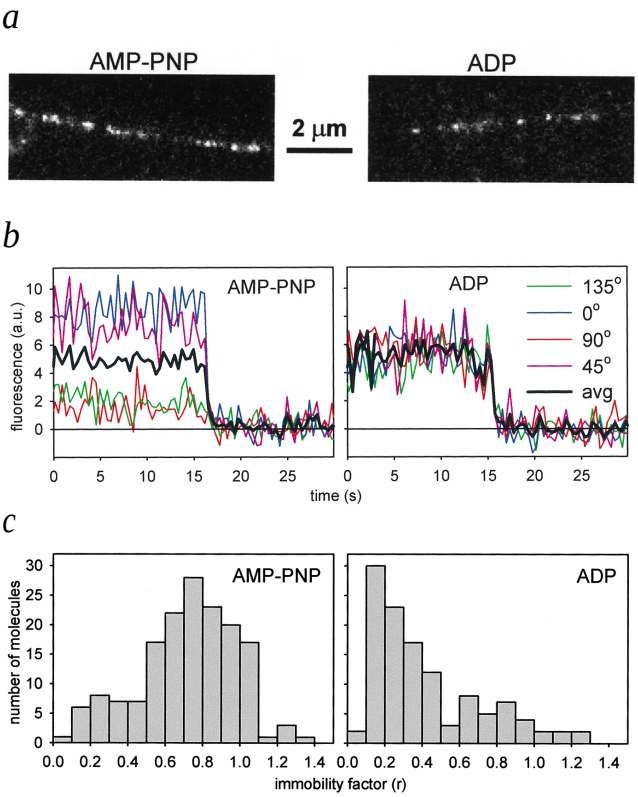

Fig. 3 Fluorescence polarization from single molecules. ***a***, Images of axonemes sparsely decorated with KMC2–BSR in the presence of AMP-PNP and ADP. ***b***, Fluorescence intensity (arbitrary units) records from single molecules. These records correspond to the time course of the emitted intensity of a fluorescent spot like the ones present in (*a*) for each polarization direction of the exciting light. The intensities (arbitrary units) of the measured molecules have a single peak distribution (AMP-PNP: mean = 4.7, s.d. = 2.5, n = 161; ADP: mean = 3.6, s.d. = 2.3, n = 117). The intensity records show a single photobleaching event and that their values have a single peak distribution, indicating that they come from single molecules. ***c***, Distribution of r values for single fluorescent molecules in the presence of AMP-PNP and ADP. The r value measures the immobility of the individual fluorophore.

on the other hand will have smaller values for both PR measures, resulting in r < 1; thus, r may be interpreted as a measure of immobility. We used this property to compare the amount of mobility in the presence of AMP-PNP and ADP. Histograms of the distribution of r values (Fig. 3*c*) show that the distribution has much lower r values (mean = 0.38, n = 117) in the presence of ADP than with AMP-PNP (mean = 0.68, n = 161). This result indicates that in the presence of ADP the probe has become more mobile — that is, dynamically disordered on the 100 ms time scale of the measurement. Therefore, the loss of polarization anisotropy of the axonemes decorated with many KMC2–BSR molecules results from the probes becoming highly mobile and not from static disorder or shifting the axial angle closer to 54.7°.

Even though the kinesin–ADP state is considered to be the one with the weakest attachment to microtubules[17], we believe that our measured kinesin molecules are attached to the axonemal microtubules because: (i) they come from aligned spots (Fig. 3*a*), and (ii) their r distribution is different from that for kinesin molecules stuck to the glass (mean = 0.52, n = 144 and mean = 0.51, n = 41 in the presence of ADP and AMP-PNP, respectively).

The dynamically disordered ADP state of KMC2–BSR could result from either a higher mobility of the kinesin loop where the probe is attached or the whole kinesin motor becoming mobile while still attached to the microtubule by a flexible link. Placing probes at different locations could help to distinguish between these two alternatives. However, in all kinesin atomic structures solved, the region where we attached the probe is highly ordered with relatively low B-factors[18] despite ADP being in the active site. These results argue against the localization of the ADP-induced increased mobility to the loop where we attached the probe. Repeated binding and dissociation of KMC2–BSR to the axonemes is also unlikely to cause the observed mobility. A KMC2–BSR molecule released from the axoneme for any significant fraction of the measurement time would diffuse away from the measured region. Thus, we favor the interpretation that the whole motor domain in the presence of ADP becomes mobile while still attached to the microtubule. Our results for the ADP state disagree with previous cryo-electron microscopy data interpreted as evidence for similar configurations for the microtubule attached motor domain in several nucleotide states including ADP[2,14,15]. However, a disordered state, like the one we detect, would be missed by averaging methods that rely on many molecules having equivalent configurations.

The flexible, mobile link between motor and track

What part of the motor domain might mediate this mobile link? Obvious candidates are the flexible loops present at the kinesin–microtubule interface. The C-terminal end of tubulin is near the kinesin binding site and is disordered in the crystal structure[19]. This part of the tubulin molecule has been proposed to mediate the link between a particular type of kinesin motor (KIF1A) and microtubules, allowing the KIF1A motor to move by a biased, one-dimensional diffusion mechanism[20]. In keeping with the proposal that specific elements of KIF1A are responsible for this particular mechanism, our single-molecule records did not show one-dimensional diffusion of KMC2–BSR during the mobile ADP state. Another disordered element that could form the flexible link between the microtubule and kinesin is loop 11 on the kinesin motor domain[12]. Located at the kinesin–microtubule interface[13], this loop is disordered in the kinesin crystal structure but is ordered in the minus-end directed motor, ncd[21]. We propose that these flexible loops in kinesin and tubulin in the ADP state mediate some of the contacts between kinesin and the microtubule. The loop flexibility might allow the whole motor to move back and forth between different configurations.

Evidence for a flexible link between a motor and its track is also present in the actomyosin system[22,23], suggesting a common occurrence in the chemomechanical cycle of motor proteins. This flexible interaction may allow the motor to initiate contact with its track even when the motor is in an unfavorable position — for example, due to the binding of the partner motor head in the kinesin dimer (Fig. 4*b*, states 2 and 3) or to position mismatches in the muscle actomyosin lattice. Also, a transition between this state and a stereo specific attachment may produce forward motion (Fig. 4*b*, state 3–4) in addition to the one associated with the movement of the neck linker (kinesin) (Fig. 4) or lever arm (myosin). There is evidence for subelemental steps from micromechanical experiments[24,25], and recent models consider the presence of two steps in the

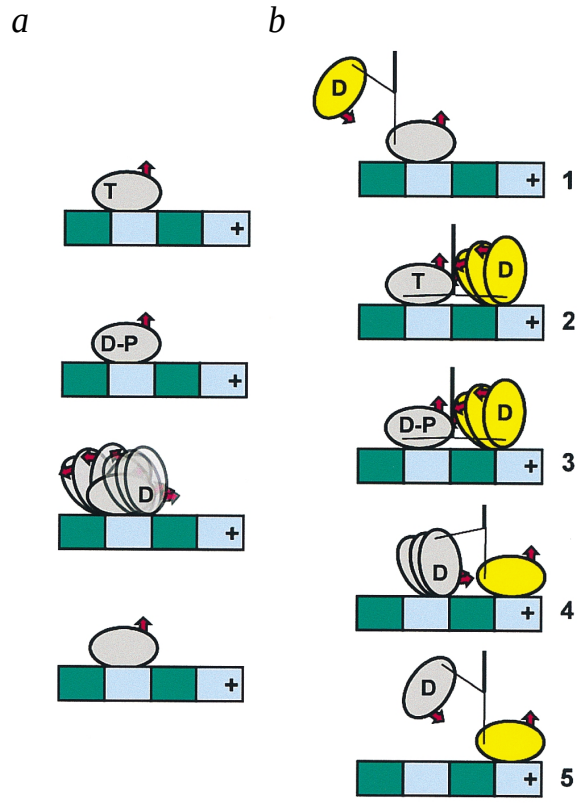

Fig. 4 Proposed structural states of kinesin. ***a***, Conformations of monomeric kinesin bound to microtubules in the different nucleotide states. In the ATP (T) and ADP-Pi (D-P) states the motor head is rigidly attached to the microtubule; after Pi release the attachment to the microtubule becomes flexible in the ADP (D) state. After ADP release the motor enters the no-nucleotide state (no letter), and the microtubule attachment becomes rigid again. The probe position and orientation is indicated by the red arrow; α and β tubulin are represented respectively in dark and light blue. ***b***, Hypothetical sequence of stepping events of a dimeric kinesin motor. Without endorsing any particular kinetic scheme, this model is presented only to show how the structural states we measured may contribute to the kinesin translocation mechanism. A previously proposed conformational change that moves the nonattached head forward after ATP binding[2] is included in the model (state 1 to 2). In states 2 to 3 the mobile ADP state helps the leading head (yellow) to find a tubulin binding site in the forward direction. From state 3 to 4 the leading head (yellow) releases ADP, enters the rigid state, pulls the trailing head (gray) and moves the linkage between the heads forward. From state 4 to 5 the trailing head (gray) with ADP detaches from the microtubule.

kinesin chemomechanical cycle[26]. We propose that for kinesin, the structural difference observed between ADP and other nucleotide states identifies a substep in the translocation cycle.

Methods

Proteins and labeling. We made a two-cysteine kinesin construct, KMC2, by modifying a pET23b plasmid containing the coding sequence of the first 349 amino acids of the human kinesin heavy chain gene (KIF5B) with a His_6-tag at the protein C-terminal end. Of the nine naturally occurring Cys residues, eight were replaced by Ala residues, leaving Cys 174. An extra Cys was introduced to replace Thr 169. This construct was expressed in *Escherichia coli* BL21 cells, and the KMC2 protein was purified by Ni-NTA agarose chromatography.

KMC2 was labeled with the bifunctional thiol reactive fluorophore bis-((N-iodoacetyl)piperazinyl) sulfonerhodamine (BSR) (Molecular Probes). Labeling was done overnight at 4 °C in 80 mM 1,4-Piperazinediethanesulfonic acid (PIPES), pH 6.8, 2 mM $MgCl_2$, 1 mM EGTA, 50 μM ATP and a 1:1 molar ratio KMC2:BSR. The reaction was stopped by adding 1 mM dithiothreitol (DTT), and the unreacted dye was removed by passing the labeled protein through a desalting column. We estimated that 60–75% of the protein was labeled with BSR. The KMC2–BSR showed normal microtubule-activated ATPase activity (V_{max} = 55 ATP s^{-1} $head^{-1}$, K_mMT = 0.5 μM in 12 mM PIPES, pH 6.8, 2 mM $MgCl_2$, 1 mM EGTA, 0.5 mM ATP). We verified by mass spectrometry that BSR reacted with KMC2 to yield one fluorophore per KMC2 molecule. Overnight digestion of KMC2–BSR with endoproteinase Lys-C, followed by liquid chromatography mass spectroscopy (LC-MS), showed a product with mass corresponding to a peptide with the two Cys residues linked to the BSR probe (predicted mass: 2,884.148 Da, experimental mass: 2,884.15 Da). Digestion with trypsin (for which there is a cleavage site at residue Arg between the cysteines) resulted in a product with mass corresponding to the two cysteine-containing peptides hydrolyzed at the middle Arg residue (expected mass increment of 18 Da for hydrolysis) but still joined by the probe crosslink (predicted mass: 2,902.15 Da, experimental mass: 2,902.45 Da). These protease digestion/LC-MS experiments confirmed that each of the two functional groups of BSR was linked to a Cys residue on KMC2. Axonemes were prepared from sea urchin sperm[27].

Fluorescence polarization microscopy. Axonemes were mixed with KMC2–BSR molecules, placed between two coverslips and observed (within a 20–30 min period). The experimental solution is 12 mM PIPES, pH 6.8, 2 mM $MgCl_2$, 1 mM EGTA, 10 mM glucose, 0.1% (v/v) β-mercaptoethanol, 0.1 mg ml^{-1} catalase, 0.03 mg ml^{-1} glucose oxidase and 7.5 mg ml^{-1} BSA. Nucleotides were added depending on the experimental conditions to be tested (AMP-PNP: 2 mM AMP-PNP; ADP: 2mM ADP; ADP–AlF_4^-: 4mM ADP, 2 mM $AlCl_3$, 10 mM KF; no-nucleotide: 5 units ml^{-1} apyrase with no added nucleotide). KMC2–BSR protein concentration was 75 nM in the multiple-molecules experiments (Fig. 2) and 0.75 nM in the single-molecule ones (Fig. 3). The axonemes decorated with KMC2–BSR protein were imaged by wide field epifluorescence (objective: Nikon 100×, 1.4 NA, PlanApo, oil immersion) (Fig. 2*a*). Laser light excitation (λ = 532 nm) was linearly polarized in different transverse directions in the plane of the microscope stage with an electro-optic modulator (EOM). The emitted light was imaged *via* a dichroic mirror (Chroma, DR540LP or DR545LP), a bandpass filter (Chroma, 570DF40), a 532 nm notch filter (Kaiser, supernotch 532) and a 4× relay lens on an intensified, frame-transfer CCD camera (I-Pentamax, Roper Scientific). After reflecting from the dichroic mirror, the intensity polarization ratios were 45:1, 18:1, 390:1 and 33:1 for the 0°, 45°, 90° and 135° cases, respectively. When four polarization axes were used, a λ / 4 plate (Tower Optical) was placed after the EOM, and two identical dichroic mirrors with planes of reflection perpendicular to each other were used to partially compensate phase distortions introduced by a single dichroic (R. Hochstrasser, pers. comm.). Sequences of images were recorded with the intensified CCD camera synchronized to the EOM to collect images with alternate polarization directions every 100 ms. To calculate the PR the emitted intensity for each polarization excitation axis was averaged first over the time period before bleaching (average = 5 s), and then the PR was calculated from the intensity averages.

Fluorophore axial angle. We derived an expression to calculate the PR of an ensemble of fluorophores bound to an axoneme with cylindrical symmetry. For this we assumed that the total light emitted by each fluorophore is proportional to the light absorbed by the fluorophore ($I_e \propto I_a \propto \cos^2\theta$, where θ is the angle the absorption dipole makes with the excitation light polarization axis). We then integrated for all fluorophores within a solid cone of semi angle Γ, which represents the mobility of the fluorophore with respect to the protein to which it is attached, and around the surface of a cone of semi angle β, the average axial angle the dipole makes with the axoneme long axis, to account for the cylindrical symmetry of binding sites on the axoneme. The resulting equation relates the PR to the angle ω of the axoneme with the x-axis

(defined as the left-right direction in the plane of the microscope sample stage), the dipole axial angle β and the mobility cone semi angle Γ:

$$PR_{0-90}(\Gamma,\beta,\omega) = -3\cos(2\omega) / \{1 + 8 / ((3\cos^2\beta - 1)(\cos\Gamma + \cos^2\Gamma))\}$$

To estimate the mobility cone semi angle Γ, we used the mobility factor r determined from single-molecule measurements. To estimate the relationship between the r factor and the semi angle Γ we calculated the average r factor from a simulation of 2,000 randomly oriented dipoles (uniformly distributed among all possible orientations in three dimensions) that were allowed to rotate freely within a cone with half angle Γ (assuming the dipole samples each position within the cone with equal probability within the measurement time). The simulations for different values of Γ showed that that an average r factor of 0.7, as in the AMP-PNP case (Fig. 3c), corresponds to a Γ value of 32°. An r factor of 0.38 as we found for the ADP state corresponds to a Γ value of 53°.

Acknowledgments

We thank R. Sakowicz for axoneme preparations, advice and discussions; R. Dickson, R. Vale and D. Pierce for their advice in the initial phases of this project; L. Gross, H. Deng and L. Siconolfi-Baez for mass spectrometry analysis; A. Asenjo for biochemical assays, and S. Brasselet and B. Lounis for helpful discussions and experimental suggestions. L.S.B. Goldstein is an investigator of the Howard Hughes Medical Institute. This project was supported by NSF grants.

Correspondence should be addressed to H.S. *email: hsosa@aecom.yu.edu*

Received 10 November, 2000; accepted 27 March, 2001.

1. Goldstein, L.S.B. & Philp, A.V. *Annu. Rev. Cell Dev. Biol.* **15**, 141–183 (1999).
2. Rice, S. *et al*. *Nature* **402**, 778–784 (1999).
3. Svoboda, K., Schmidt, C.F., Schnapp, B.J. & Block, S.M. *Nature* **365**, 721–727 (1993).
4. Rosenfeld, S.S., Correia, J.J., Xing, J., Rener, B. & Cheung, H.C. *J. Biol. Chem.* **271**, 30212–30221 (1996).
5. Moerner, W.E. & Orrit, M. *Science* **283**, 1670–1676 (1999).
6. Weiss, S. *Science* **283**, 1676–1683 (1999).
7. Lu, H.P., Xun, L. & Xie, X.S. *Nature* **282**, 1877–1882 (1998).
8. Ha, T., Laurence, T.A., Chemla, D.S. & Weiss, S. *J. Phys. Chem. B* **103**, 6839–6850 (1999).
9. Adachi, K. *et al*. *Proc. Natl. Acad. Sci. USA* **97**, 7243–7247 (2000).
10. Warshaw, D.M. *et al*. *Proc. Nat. Acad. Sci. USA* **95**, 8034–8039 (1998).
11. Corrie, J.E.T. *et al*. *Nature* **400**, 425–430 (1999).
12. Kull, F.J., Sablin, E.P., Lau, R., Fletterick, R.J. & Vale, R.D. *Nature* **380**, 550–555 (1996).
13. Sosa, H. *et al*. *Cell* **90**, 217–224 (1997).
14. Arnal, I. & Wade, R.H. *Structure* **6**, 33–38 (1998).
15. Hirose, K., Lowe, J., Alonso, M., Cross, R.A. & Amos, L.A. *Mol. Biol. Cell* **10**, 2063–2074 (1999).
16. Funatsu, T., Harada, Y., Tokunaga, M., Saito, K. & Yanagida, T. *Nature* **374**, 555–559 (1995).
17. Ma, Y.Z. & Taylor, E.W. *J. Biol. Chem.* **272**, 724–730 (1997).
18. Sack, S., Kull, F.J. & Mandelkow, E. *Eur. J. Biochem.* **262**, 1–11 (1999).
19. Nogales, E., Whittaker, M., Milligan, R.A. & Downing, K.H. *Cell* **96**, 79–88 (1999).
20. Okada, Y. & Hirokawa, N. *Science* **283**, 1152–1157 (1999).
21. Sablin, E.P., Kull, F.J., Cooke, R., Vale, R.D. & Fletterick, R.J. *Nature* **380**, 555–559 (1996).
22. Taylor, K.A. *et al*. *Cell,* **99**, 421–431 (1999).
23. Walker, M., Zhang, X.Z., Jiang, W., Trinick, J. & White, H.D. *Proc. Nat. Acad. Sci. USA* **96**, 465–470 (1999).
24. Coppin, C.M., Finer, J.T., Spudich, J.A. & Vale, R.D. *Proc. Nat. Acad. Sci. USA* **93**, 1913–1917 (1996).
25. Veigel, C. *et al*. *Nature* **398**, 530–533 (1999).
26. Schnitzer, M.J., Visscher, K. & Block, S.M. *Nature Cell Biol.* **2**, 718–723 (2000).
27. Gibbons, I.R. & Fronk, E. *J. Biol. Chem.* **254**, 187–196 (1979).
28. Kozielski, F. *et al*. *Cell* **91**, 985–994 (1997).
29. Kozielski, F., Arnal, I. & Wade, R.H. *Curr. Biol.* **8**, 191–198 (1998).
30. van Amerongen, H. & Struve, W.S. *Methods Enzymol.* **246**, 259–283 (1995).